LOW-FREQUENCY PASSIVE NOISE CONTROL USING PERIODIC HELMHOLTZ RESONATOR ARRAYS

Wanderson V. O. Monteiro[1], José M. C. dos Santos[1], Edilson D. Nóbrega[2]

[1]*Dept. Computational mechanics, University of Campinas*
Rua Mendeleyev 200, Cidade Universitária Zeferino Vaz, Campinas - SP, Brazil
w203198@dac.unicamp.br, zema@fem.unicamp.br
[2]*Dept. Mechanical engineering, Federal University of Maranhão,*
Cidade Universitária Dom Delgado, São Luís - MA, Brazil
edilson.dantas@ufma.br

Abstract. Passive noise control in specific frequency ranges can be achieved using Helmholtz resonators (HR), which are reactive devices that exhibit distinctive geometry, resulting in impedance variations within the enclosing system. Due to the acoustic resonance in the HR, such variations enable the attenuation of propagating waves within a narrow frequency range. When multiple HRs are periodically arranged in an acoustic system, they produce an acoustic metamaterial that greatly expands the frequency range known as a stop band or band gap, which are band structures where sound waves are not allowed to propagate or attenuated. The aim of this paper is to analyze sound wave attenuation in an acoustic metamaterial consisting of HRs arranged in parallel and in series configurations. For this purpose, methods such as the transfer matrix and conventional finite elements will be employed. Parameter sensitivity analysis of HR geometry will be conducted to maximize the attenuation bandwidth of band gaps through Differential Evolution. An optimization process is also conducted to obtain the best sound attenuation using metrics such as sound transmission loss through the amplitude of the incident and reflected wave. Simulated examples are presented to demonstrate the efficiency and validation of the proposed methods.

Keywords: Passive noise control, Helmholtz resonators, Acoustic metamaterial, Band gap, Differential evolution.

1 Introduction

In the context of engineering structures, various systems such as ventilation ducts, heat exchanger tubes, and steam supply ducts often generate unwanted noise due to fluid flow inside them [1]. The control of these noises can be achieved through active approaches, electronic devices, or passive approaches, through more traditional solutions like silencers. Reactive silencers passive, such as Helmholtz Resonators (HR) or expansion chambers, have stood out for delivering effective noise control results, and they are also more financially accessible options.

However, HRs reveal a disadvantage as they only attenuate noise within a narrow frequency range [2]. In other words, they exhibit a high sound transmission loss at their resonance frequency [3]. Nevertheless, the attenuation bandwidth of these devices is notably limited, which is directly associated with the geometry of the resonator. A considerable volume of their cavity is necessary to achieve attenuation at low frequencies using HRs, making their application impractical in many engineering scenarios [4].

Recently, studies have emerged that address periodically designed structures and materials, known as phononic crystals or metamaterials. These new structures are implemented in various structural elements such as bars, beams, plates, and shells, with the aim of controlling vibration in different systems [5–8]. When applied to acoustic control, these structures, called acoustic metamaterials, stand out for utilizing silencers, such as expansion chambers, micro-perforated panels, Helmholtz resonators, side-branch ducts, and metasurfaces, as fundamental components of their applications [9–11].

An additional approach for noise control involves using systems composed of multiple Helmholtz resonators. In this context, these HRs are distributed periodically along the longitudinal direction of the duct, forming a transverse array with several distinct resonance frequencies. This configuration aims to enhance the efficiency of

the acoustic control system, broadening the range of sound attenuation compared to individual resonators [12–14]. The combination of these technologies has been of great interest in the engineering community, as they significantly reduce noise impact in operational environments. This improves the quality of work and users' comfort while meeting regulatory requirements related to industrial noise control.

One of the main methods used to investigate wave propagation in periodic structures is the Transfer Matrix Method (TMM), which establishes a relationship between the input and output of acoustic systems. Aligned with Bragg's theory, TMM allows for obtaining various attenuation bands in sound transmission loss. This effect results from the local resonance of HRs and Bragg scattering caused by the interaction between incident and reflected waves within the duct, due to the spatial periodicity configuration. The appearance of forbidden bands in the dispersion diagram indicates the regions of sound attenuation in the system.

Differential Evolution (DE) is an optimization technique based on evolutionary processes to solve optimization problems. Initially proposed by Storn and Price [15], this approach has become widely used in various areas, including optimizing metamaterials and phononic crystals. DE has proven to be applicable to metamaterial optimization, serving as a tool to find optimal combinations of parameters. Through evolution, DE efficiently explores the parameter space, adjusting the geometry or physical characteristics of metamaterials to achieve the desired performance. This is particularly advantageous when multiple objectives exist, such as maximizing sound absorption at different frequencies [16, 17].

In this study, we investigated wave propagation in an acoustic metamaterial composed of multiple HRs using the Transfer Matrix Method to obtain sound transmission loss through the amplitudes of incident and reflected waves within the system. The results were compared with three-dimensional simulations conducted using the finite element method with the commercial software COMSOL. Subsequently, we employed the DE algorithm to widen the bandwidth of sound attenuation, transforming the system into an efficient acoustic controller capable of providing attenuation at low frequencies and a broad range of sound attenuation.

2 Multiple Helmholtz resonator arrays

Figure 1a depicts the HR model, which is divided into three parts: the volume of the resonator, the neck, and the main duct. In this model, a final correction is applied to enhance its approach, and Fig. 1b illustrates multiple HRs arranged periodically around and along the duct

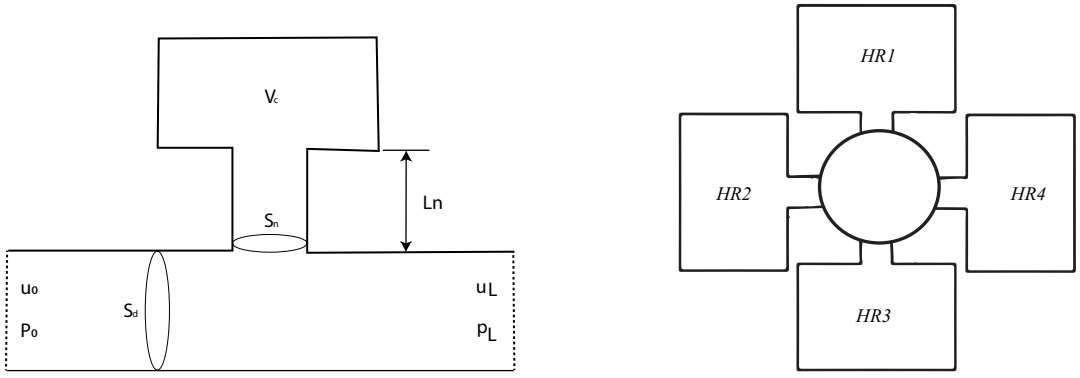

(a) HR model parameters. (b) Front view.

Figure 1. HR Model: Parameters and frontal view visualization.

Where S_d is the area of the main duct, S_n is the area of the neck, l_n is the length of the neck, and $V_c = \pi r_c^2 l_c$ is the volume of the cavity, with r_c as cavity radius and l_c as cavity height. The correction for the neck length is given by: $l'_n = l_n + 1.7 \cdot r_n$, where r_n is the radius of the neck [18]. The acoustic impedance adopted for the HR is [13]:

$$Z_r = j\left(\omega \frac{\rho_0 l'_n}{S_n} - \frac{1}{\omega}\frac{\rho_0 c_0^2}{V_c}\right). \tag{1}$$

They consider ω as the angular frequency, and ρ_0 and c_0 as the density and speed of sound, respectively. Each cell consists of a uniform part of the duct associated with the resonators, where the internal diameters remain constant throughout the structure, with d being the length of each cell.

Sound pressure, P_n, and the particle velocity, u_n, in each periodic cell are given by:

$$\begin{aligned} P_n(x) &= I_n e^{-jk(x-x_n)} + R_n e^{jk(x-x_n)} \\ u_n(x) &= \frac{I_n}{\rho_0 c_0} e^{-jk(x-x_n)} - \frac{R_n}{\rho_0 c_0} e^{jk(x-x_n)}, \end{aligned} \tag{2}$$

where k represents the wave number, j is the imaginary unit, and x_n denotes the center of the uniform duct. Additionally, I_n and R_n are the complex amplitudes of the incident and reflected waves, respectively. When considering four transverse resonators, as shown in Figure 1b, we obtain the equivalent impedance $Z_{he} = Z_{r1}Z_{r2}Z_{r3}Z_{r4}/(Z_{r1}Z_{r2}Z_{r3}+ Z_{r1}Z_{r2}Z_{r4} + Z_{r1}Z_{r3}Z_{r4} + Z_{r2}Z_{r3}Z_{r4})$ in multiples of HRs. By considering the continuity condition of sound pressure and particle velocity, with $x_n = (n-1)d$ and $x = nd$, as described in [13], it has:

$$\begin{bmatrix} I_{n+1} \\ R_{n+1} \end{bmatrix} = \underbrace{\begin{bmatrix} e^{(-jkd)} & 0 \\ 0 & e^{(jkd)} \end{bmatrix} \times \begin{bmatrix} (1-\rho_0 c_0/2S_d Z_{he}) & -\rho_0 c_o/2S_d Z_{he} \\ rho_0 c_0/2S_d Z_{he} & (1+\rho_0 c_0/2S_d Z_{he}) \end{bmatrix}}_{\mathbf{T}_p} \begin{bmatrix} I_n \\ R_n \end{bmatrix}, \tag{3}$$

where $\mathbf{T_p}$ is the transfer matrix relating the wave amplitudes. The amplitudes of incident and reflected waves can be obtained through the eigenvectors ($\mathbf{\Phi}$) and eigenvalues ($\mathbf{e}^{\mu}$) of the matrix $\mathbf{T_p}$:

$$\begin{Bmatrix} I_{n+1} \\ R_{n+1} \end{Bmatrix} = \mathbf{T}_p^1 \begin{Bmatrix} I_n \\ R_n \end{Bmatrix} = \mathbf{T}_p^2 \begin{Bmatrix} I_{n-1} \\ R_{n-1} \end{Bmatrix} = \dots \mathbf{T}_p^n \begin{Bmatrix} I_1 \\ R_1 \end{Bmatrix} = a e^{\mu^+ n} \begin{Bmatrix} \Phi_I^+ \\ \Phi_R^+ \end{Bmatrix} + b e^{\mu^- n} \begin{Bmatrix} \Phi_I^- \\ \Phi_R^- \end{Bmatrix}. \tag{4}$$

The coefficients a and b are determined by the boundary conditions. The superscripts $+$ and $-$ indicate the forward-going ($+x$ direction) and backward-going ($-x$ direction) waves, respectively. When $|\Phi_I/\Phi_R| > 1$, the Bloch wave displaces in the positive direction, while for $|\Phi_I/\Phi_R| < 1$, the displacement occurs in the negative direction. Here, $\mu = -jk_B h$ corresponds to the attenuation coefficient, where k_B is the Bloch wave number. The transmission loss of the n-th can be calculated as:

$$STL = 20\log\left|\frac{I_1}{I_{n+1}}\right| = \left|\frac{a\Phi_I^+ + b\Phi_I^-}{ae^{\mu^+ n}\Phi_I^+ + be^{\mu^- n}\Phi_I^-}\right|. \tag{5}$$

Considering an anechoic termination ($R_{n+1} = 0$), Eq. (5) can be reduced to [13]:

$$STL = -20(n+1)log_{10}|e^{\mu^+}|. \tag{6}$$

3 Simulated results and discussion

Figure 2a illustrates the periodic structure with transverse HR obtained by TMM and FEM (Comsol software). Figure 2b shows the FEM mesh used to obtain the results.

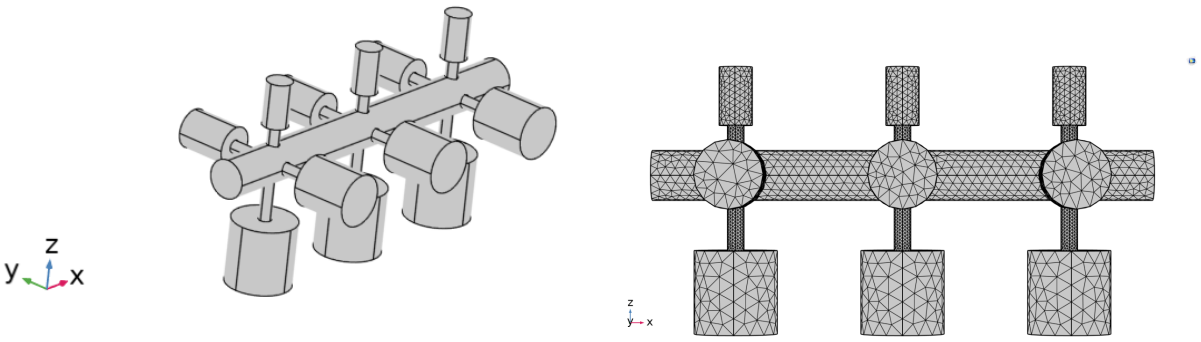

(a) Multiple Helmholtz resonator arrays on the duct. (b) Applied mesh.

Figure 2. Multiple Helmholtz Resonator arrays and applied FEM mesh.

The parameters used for the transverse HRs were as follows: air speed of sound, $c_0 = 343$ m/s, air mass density, $\rho_0 = 1.2031$ kg/m^3, duct cross-section area, $S_d = 0.0009\pi$ ^{2}, tube diameters $r_{n1} = r_{n2} = r_{n3} = r_{n4} =$

0.01 m, neck lengths $l_{n1} = 0.03$ m, $l_{n2} = 0.04$ m, $l_{n3} = 0.05$ m, and $l_{n4} = 0.06$ m, duct length $d = 0.2$ m, and chamber volumes $V_{c1} = 2.80 \times 10^{-5}\pi\ m^3$, $V_{c2} = 7.20 \times 10^{-5}\pi\ m^3$, $V_{c3} = 1.44 \times 10^{-4}\pi\ m^3$, and $V_{c4} = 2.5 \times 10^{-4}\pi\ m^3$.

Figure 3a and 3b present the results of the Sound Transmission Loss (STL) for a single-cell and three cells model obtained by the Transfer Matrix Method (TMM) and the Finite Element Method (FEM) (COMSOL software), respectively, where a good approximation is observed. Band gaps and sound attenuation occur at the same frequency range. It can be observed that for larger HRs, the STL level becomes higher. Figure 3c shows the dispersion diagram, obtained from the wavenumber of the eigenvalue of the matrix $\mathbf{Tp}$, where the real part represents propagating waves, while the imaginary part shows the band gaps, frequency ranges in which the waves are attenuated. Four band gaps generated by the local resonance and one by the Bragg effect are observed for the initial model, corresponding to the HRs resonance frequency and the periodicity, respectively, demonstrating the attenuation bands in the STL.

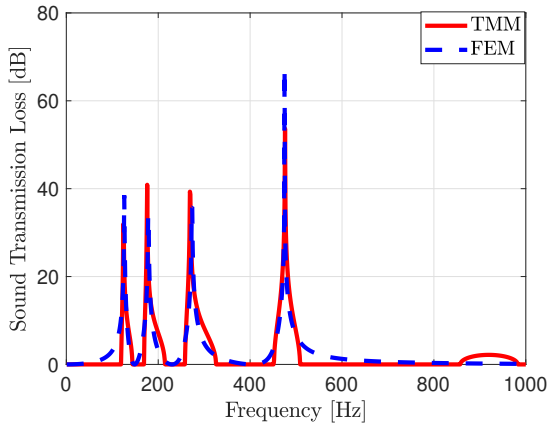

(a) Sound transmission loss to a single cell.

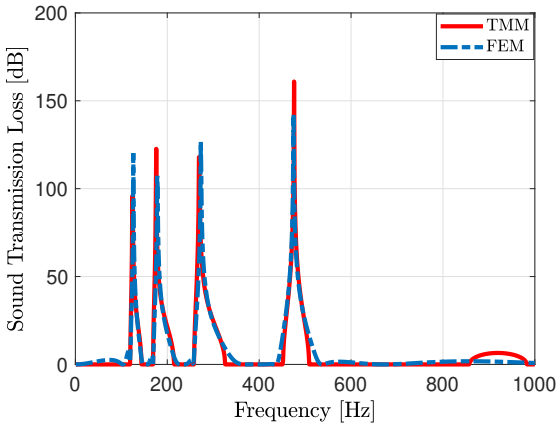

(b) Sound transmission loss for three unit cells.

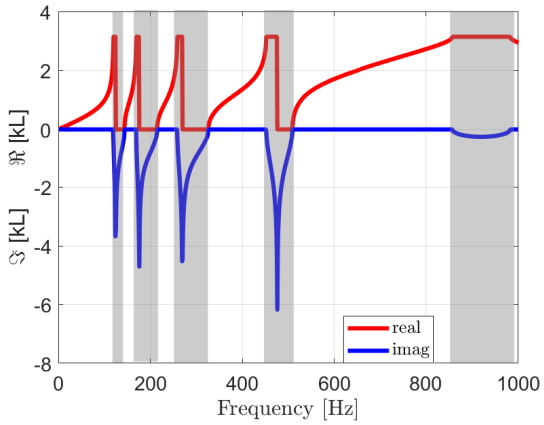

(c) Dispersion diagram.

Figure 3. STL and dispersion diagram for a periodic array of transverse resonators.

The Differential Evolution algorithm emerges as a powerful optimization tool. Inspired by natural evolution, DE employs combinations, mutations, and selection of candidate solutions to efficiently explore an extensive parameter search space for the Helmholtz resonators. In this way, it can find the most suitable combination of resonators, providing the widest possible band of attenuation in the duct at a specific frequency. Table 1 displays the maximum and minimum parameters used in the DE:

Table 1. Optimization design parameter limits.

Parameters	r_{n1}	r_{n2}	r_{n3}	r_{n4}	l_{n1}	l_{n2}	l_{n3}	l_{n4}	r_{c1}	r_{c2}	r_{c3}	r_{c4}	l_{c1}	l_{c2}	l_{c3}	l_{c4}
Minimum	0.0050	0.0050	0.0050	0.0050	0.020	0.020	0.020	0.020	0.010	0.010	0.010	0.010	0.040	0.040	0.040	0.040
Maximum	0.020	0.020	0.020	0.020	0.070	0.070	0.070	0.070	0.060	0.060	0.060	0.060	0.100	0.100	0.100	0.100

The flowchart presented in Fig. 4 depicts an outline of the Differential Evolution (DE) algorithm. The process begins with defining initial parameters, such as the population size and search parameter limits. Next, an initial population of individuals is generated, randomly selected. Afterward, the objective function is evaluated for each individual, aiming to maximize the bandwidth within the intervals of 150 to 550 Hz. The best individuals are selected to create the next generation, considering their performance achieved in the objective function.

The algorithm proceeds interactively, applying recombination and mutation operators to generate new individuals. The evaluation of the objective function is again performed for the newly generated population, and the selection, recombination, and mutation process is repeated until the maximum number of generations is reached.

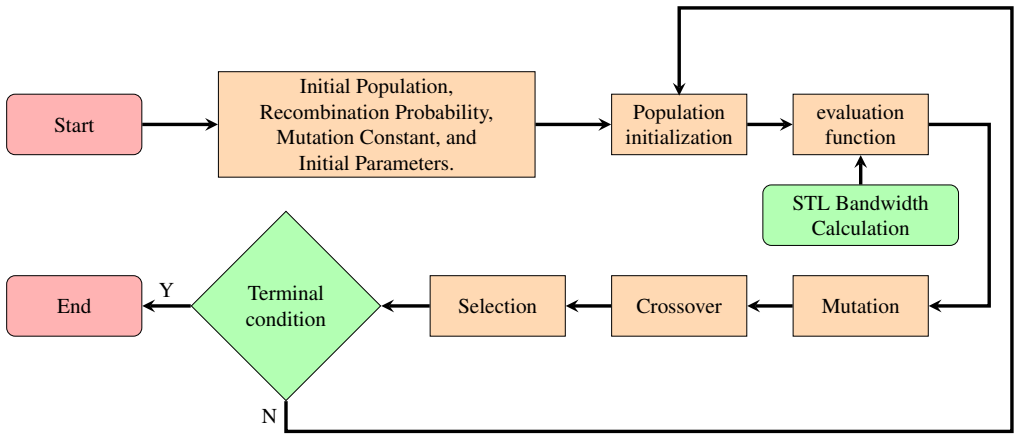

Figure 4. Differential Evolution Algorithm Flowchart

Table 2 shows the parameters of the best individuals obtained by the DE, and Fig. 5 displays the corresponding values of the Sound Transmission Loss (STL) for these parameters, together with its dispersion diagram.

Table 2. Optimization design parameters.

Parameters	r_{n1}	r_{n2}	r_{n3}	r_{n4}	l_{n1}	l_{n2}	l_{n3}	l_{n4}	r_{c1}	r_{c2}	r_{c3}	r_{c4}	l_{c1}	l_{c2}	l_{c3}	l_{c4}
Best value	0.0200	0.0184	0.0179	0.0194	0.0290	0.0646	0.0250	0.0700	0.0600	0.0493	0.0591	0.0508	0.1060	0.0738	0.1000	0.1000

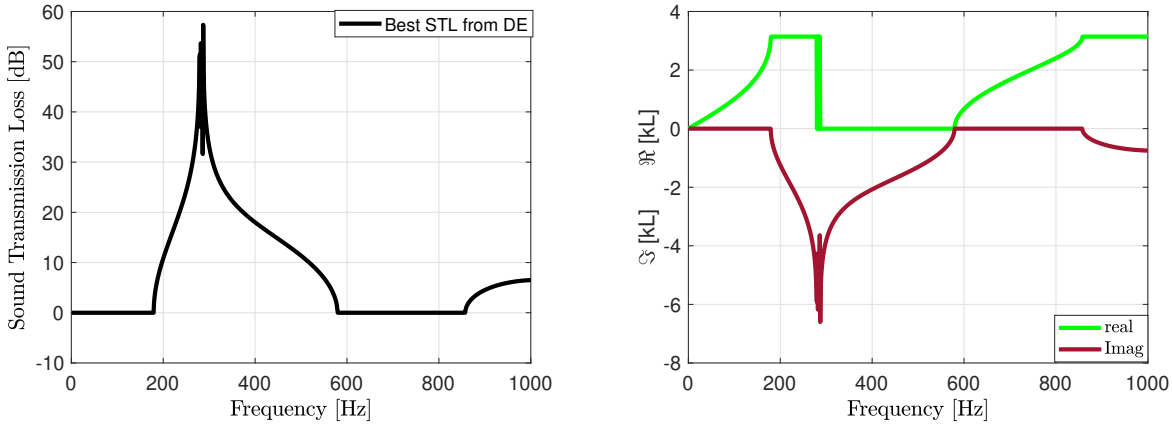

(a) Optimized sound transmission loss.

(b) Dispersion diagram of DE optimization.

Figure 5. DE optimization.

The DE algorithm obtained a parameter configuration in which the objective function exhibited continuous attenuation in the frequency range. This was achieved by overlapping the resonance frequencies of each resonator in the cell.

4 Conclusions

An acoustic metamaterial with four transverse HRs was investigated using the Transfer Matrix Method and Finite Element Method (COMSOL software). The approach involving incident and reflected wave amplitudes yielded results in agreement with the three-dimensional outcomes.

The analysis of sound transmission loss and the dispersion diagram was conducted for a single unit cell and three periodic cells, revealing that periodicity amplifies the attenuation amplitudes. Subsequently, by employing the Differential Evolution (DE) algorithm, parameters were optimized to broaden the bandwidth for low frequencies, thereby offering a potential solution to the issue of concentrated attenuation in Helmholtz resonators.

Acknowledgements. The authors are grateful to the Brazilian research funding, FAPESP (Grant No. 15894-0/2018) , CNPq (Grant No. 317436/2021-0), FAPEMA (Grant No. BM-01652/23, APP-09180/22) for the financial support.

Authorship statement. The authors hereby confirm that they are the sole liable persons responsible for the authorship of this work, and that all material that has been herein included as part of the present paper is either the property (and authorship) of the authors, or has the permission of the owners to be included here.

References

[1] D.-L. Yu, H.-J. Shen, J.-W. Liu, J.-F. Yin, Z.-F. Zhang, and J.-H. Wen. Propagation of acoustic waves in a fluid-filled pipe with periodic elastic Helmholtz resonators. *Chinese Physics B*, vol. 27, n. 6, pp. 064301, 2018.
[2] Y. Li, H. Shen, L. Zhang, Y. Su, and D. Yu. Control of low-frequency noise for piping systems via the design of coupled band gap of acoustic metamaterials. *Physics Letters A*, vol. 380, n. 29, pp. 2322–2328, 2016.
[3] S.-H. Seo and Y.-H. Kim. Silencer design by using array resonators for low-frequency band noise reduction. *The Journal of the Acoustical Society of America*, vol. 118, n. 4, pp. 2332–2338, 2005.
[4] C. CAI and C. M. MAK. Noise attenuation capacity of a helmholtz resonator. *Advances in Engineering Software*, vol. 116, pp. 60–66, 2018.
[5] A. Goto, E. Nóbrega, F. Pereira, and J. Dos Santos. Numerical and experimental investigation of phononic crystals via wave-based higher-order rod models. *International Journal of Mechanical Sciences*, vol. 181, pp. 105776, 2020.
[6] E. Nóbrega, V. Pereira, D. Costa, and J. Dos Santos. Modelling elastic phononic crystal beam via en- ergy spectral element method, 2020.
[7] F. Pereira and J. Dos Santos. Phononic crystal investigation using a fluid-structure circular cylindrical shell spectral element. *Mechanical Systems and Signal Processing*, vol. 148, pp. 107100, 2021.
[8] E. Miranda Jr, E. Nóbrega, S. Rodrigues, C. J. Aranas, and J. Dos Santos. Wave attenuation in elastic metamaterial thick plates: Analytical, numerical and experimental investigations. *International Journal of Solids and Structures*, vol. 204-205, 2020.
[9] P. Liu, S. Zuo, X. Wu, S. Chen, and Y. Kong. Acoustic attenuation characteristics of the muffler phononic crystal with hybrid resonators. *International Journal of Mechanical Sciences*, vol. 234, pp. 107677, 2022.
[10] S. Wei, L. Li, C. Zhigang, L. Linyong, and F. Xiaopeng. A parameter design method for multifrequency perfect sound-absorbing metasurface with critical coupled helmholtz resonator. *Journal of Low Frequency Noise, Vibration and Active Control*, vol. 40, n. 4, pp. 2054–2063, 2021.
[11] K. Mahesh and R. Mini. Investigation on the acoustic performance of multiple helmholtz resonator configurations. *Acoustics Australia / Australian Acoustical Society*, pp. 1–15, 2021.
[12] D. Wu and N. Zhang. The improvement on noise attenuation performance of a duct-resonator system. *Journal of Asian Architecture and Building Engineering*, vol. 16, n. 3, pp. 669–674, 2017.
[13] D. Wu, N. Zhang, C. M. Mak, and C. Cai. Hybrid noise control using multiple helmholtz resonator arrays. *Applied Acoustics*, vol. 143, pp. 31–37, 2019.
[14] Z. Zhang, D. Yu, J. Liu, B. Hu, and J. Wen. Transmission and bandgap characteristics of a duct mounted with multiple hybrid helmholtz resonators. *Applied Acoustics*, vol. 183, pp. 108266, 2021.
[15] R. Storn and K. Price. Differential evolution - a simple and efficient heuristic for global optimization over continuous spaces. *Journal of Global Optimization*, vol. 11, pp. 341–359, 1997.
[16] A. Goto and J. Dos Santos. Differential evolution optimization of periodic micro-perforated chamber mufflers for low-frequency sound attenuation, 2021.
[17] H. Zhao, Y. Wang, J. Wen, Y. W. Lam, and O. Umnova. A slim subwavelength absorber based on coupled microslits. *Applied Acoustics*, vol. 142, pp. 11–17, 2018.

[18] M. L. Munjal. *Acoustics of Ducts and Mufflers With Application to Exhaust and Ventilation System Design*. Wiley, 1 edition, 1987.